

TWO-SCALE NEURAL NETWORKS FOR PARTIAL DIFFERENTIAL EQUATIONS WITH SMALL PARAMETERS

QIAO ZHUANG, CHRIS ZIYI YAO, ZHONGQIANG ZHANG, AND GEORGE EM KARNIADAKIS

ABSTRACT. We propose a two-scale neural network method for solving partial differential equations (PDEs) with small parameters using physics-informed neural networks (PINNs). We directly incorporate the small parameters into the architecture of neural networks. The proposed method enables solving PDEs with small parameters in a simple fashion, without adding Fourier features or other computationally taxing searches of truncation parameters. Various numerical examples demonstrate reasonable accuracy in capturing features of large derivatives in the solutions caused by small parameters.

1. INTRODUCTION

In this work, we consider physics-informed neural networks (PINNs) for the following equation

$$(1.1) \quad d\partial_t u - \varepsilon L_2 u + L_0 u = f, \quad \mathbf{x} \in D \subset \mathbb{R}^d,$$

where some proper boundary conditions and initial conditions are imposed. Here $d = 0$ or 1 and $\varepsilon > 0$. Also, $L_2 u$ consists of the leading-order differential operator and $L_0 u$ consists of lower-order linear or nonlinear differential operators. For example, consider a singular perturbation problem where $d = 0$, $L_2 u = \operatorname{div}(a \nabla u)$ is second-order and $L_0 u = b \cdot \nabla u + cu$ is first-order.

Small parameters in the equation often pose extra difficulties for numerical methods, see e.g., [27]. The difficulties come from one or more sharp transitions in regions of small volumes, which implies large first-order derivatives or even large high-order derivatives. When $d = 0$, $\varepsilon > 0$ is very small, $L_2 u = \Delta u$ and $L_0 u = \mathbf{1} \cdot \nabla u$, then at least one boundary layer arise.

When deep feedforward neural networks are used, they are usually trained with stochastic gradient descent methods but do not resolve the aforementioned issues as they learn functions with low frequency and small first-order derivatives, see e.g., in [3, 26, 38].

1.1. Literature review. To deal with functions with high-frequency components such as in singular perturbation problems, at least four approaches have been proposed to address this issue:

- Adding features in the neural networks: Adding random Fourier features is probably the most non-intrusive approach. Adding $\cos(\omega_i^\top x)$, $\sin(\omega_i^\top x)$'s to deep neural networks as approximations of target functions or solutions. With an explicitly specified range for the random frequencies, one can learn a large class of functions. In [31, 20, 18, 5], frequency ranges are scheduled to represent complicated solutions to partial differential equations. See also [39, 19, 42] for more elliptic type multi-scale PDEs. The Fourier feature networks are also used in [34, 35], and see [33] for a review.
- Enhanced loss by adding first-order and higher-order derivatives: Another approach is to include the gradient information in the loss function, e.g., in [6, 12, 17]. This approach has been applied to solve partial differential equations, e.g., in [28, 40].
- Adaptive weights: In the loss function, adaptive weights are assigned to have a better balance of each squared term in the least-squares formulation, e.g., self-adaptive [24], attention-based weights [2], binary weights [10]. See also [37, 41, 23].

Date: February 28, 2024.

Keywords: two-scale neural networks, partial differential equations, small parameters

- **Resampling:** Sampling points in the loss function can be made adaptive based on the residuals at sampling points during the training process such as in [21, 36, 9, 8]. Also, in [25, 29, 30], the density function for sampling during the training is computed using the idea of importance sampling. The density function for re-sampling is approximated by Gaussian mixtures and formulated by finding the min-max of the loss function via fixed-point iterations.

Other approaches are not particularly for the high-frequency issue, such as [14] using adaptive activation functions and [32] by respecting causality.

1.2. Related works. One relevant approach to accommodate multiple scales using neural networks is the asymptotic-preserving neural network (APNN) [15, 22, 4]. It involves two-scale expansions and transforming the underlying equation into several equations that may be scale-independent. For example, in [15, 22], the loss function is designed based on equations from a macro-micro decomposition, while in [4], the loss function is rooted in a system in a macroscopic form that corresponds to the governing PDEs. In [11], dimension-augmentation is used to enhance the accuracy, which includes adding the Fourier features. Our approach is closely related to APNN as we explicitly build-in a scale as an extra dimension of input for the neural networks. Another relevant approach is multi-level neural networks [1], addressing the multiple scales in the solution by using a sequence of neural networks with increasing complexity: at each level of the process, it uses a new neural network, to generate a correction corresponding to the error in the previous approximation. Two ingredients are essential in mitigating the effects of high-frequency components: adding Fourier features in the networks and the extra level of refining residuals. A similar approach is in [7] while the scale of residuals is not explicitly incorporated in the solution.

1.3. Contribution and significance of the work. We directly incorporate the scale parameter into the neural networks' architecture, establishing a two-scale neural network method. In particular, for a small scale parameter ϵ , the networks employ auxiliary variables related to the scale of ϵ^γ ($\gamma \in \mathbb{R}$) designed to capture intricate features that involve large derivatives such as boundary layers, inner layers, and oscillations. Specifically, we use the feedforward neural network of the form

$$(1.2) \quad w(\mathbf{x})N(\mathbf{x}, \epsilon^\gamma(\mathbf{x} - \mathbf{x}_c), \epsilon^\gamma),$$

where $\mathbf{x}_c \in D$. Here $w(\mathbf{x})$ is 1 when boundary layers arise or a simple function satisfying the Dirichlet boundary condition if no boundary layer arises. Without an explicit statement, \mathbf{x}_c is the center of the domain D . To assess the performance of the two-scale neural networks, we will compare their results with those of the following one-scale neural networks

$$(1.3) \quad w(\mathbf{x})N(\mathbf{x}).$$

The significance of this work is that the new architecture of networks enables solving problems with small parameters in a simple fashion. For example, we do not need to determine how many equations in APNN, or levels in multilevel neural networks [1], which are problem-dependent. We also avoid the use of Fourier features, a lot of which may be required in two dimensions and even higher dimensions.

We compare our method with multilevel neural networks [1], underscoring our method's capability to capture large derivatives without tuning scaling factors. The design of the two-scale neural networks enables the neural networks to implicitly pick up the scale expansions to accommodate the multiple scales. In contrast, APNN accommodate the multiple scales via explicit asymptotic expansions, resulting in decomposition strategies such as micro-macro and even-odd decomposition. The selection of decomposition strategies and truncation terms of asymptotic expansions is critical to the APNN model's outcomes. Owing to the variability these choices introduce, we refrain from using APNN results as a benchmark to be compared within our study.

The effectiveness of the proposed two-scale approach in handling large derivatives is demonstrated by comprehensive numerical examples in Section 3. These include complex cases such as problems with dual boundary layers in 1D and 2D, viscous Burgers equations, and Helmholtz equations exhibiting oscillations along xy and radial directions, where the corresponding one-scale method falls short in delivering accurate simulations without special treatments.

2. FORMULATION AND ALGORITHMS

Under the framework of PINNs, the neural network solution is obtained by minimizing the loss function of residuals. The loss function of the considered problem (1.1) at the continuous level is

$$(2.1) \quad \int_{[0,T] \times D} r^2(t, x) + \alpha \int_{\partial D} (u - g)^2 + \alpha_1 \int_D |\nabla u|^2 + \beta \cdot \text{loss of initial conditions}$$

where $\alpha \geq 1$, $\alpha_1 \geq 0$ and $\beta \geq 0$ and

$$r(t, x) = d\partial_t u - \varepsilon L_2 u + L_0 u - f.$$

The discrete formulation corresponding to (2.1) is

$$\frac{1}{N_c} \sum_{i=1}^{N_c} |r(t_r^i, \mathbf{x}_r^i)|^2 + \frac{\alpha}{N_b} \sum_{i=1}^{N_b} |u(t_b^i, \mathbf{x}_b) - g^i|^2 + \frac{\beta}{N_0} \sum_{i=1}^{N_0} |u(t_0, \mathbf{x}_0^i) - u_0^i|^2 + \frac{\alpha_1}{N_c} \sum_{i=1}^{N_c} |\nabla u(t_r^i, \mathbf{x}_r^i)|^2,$$

where $\{t_r^i, \mathbf{x}_r^i\}_{i=1}^{N_c}$ specify the collocation points in the interior time $(0, T]$ and spatial domain D , $\{t_b^i\}$ are time collocation points at $\mathbf{x} = \mathbf{x}_b$, \mathbf{x}_0^i are spacial collocation points at $t = t_0$.

In this paper, we utilize the Adam [16] optimizer to train the neural network parameters. To enhance the accuracy of capturing solutions to problems with small parameters ε , we employ a successive training strategy. This approach progressively optimizes the weights and biases of the neural networks, starting with modestly larger ε_0 as the initial guess. We summarize the successive training method in Algorithm 1.

Algorithm 1: Successive training of two-scale neural networks for PDEs with small parameters

Data: Training set, adaptive learning rates, ε and other parameters from the PDE

Result: Optimized weights and bias of the neural networks

Step 1. Pick a large ε_0 if ε is small; otherwise set $\varepsilon_0 = \varepsilon$. Train optimized weights and bias of the neural networks with the scale 1 and $\varepsilon_0^{-\frac{1}{2}}$.

Step 2. Repeat Step 1 once if necessary, e.g. 10ε is still small.

Step 3. Compute the gradients of the trained neural networks in Steps 1 & 2 on a different set of sampling points, in addition to training points.

Step 4. (Adaptive sampling). Find the first few points where the norm of the gradient is large. Add a few more points.

Step 5. (Fine-tuning). Use Adam with a smaller learning rate to further optimize the weights and biases.

Step 6. Stop the process if the iteration attains the maximal epoch number specified.

3. NUMERICAL RESULTS

In this section, we employ the two-scale neural network method for extensive numerical tests on problems where small parameters lead to solutions with large derivatives. The numerical tests cover one-dimensional (1D) ODEs with one (Example 3.1) and two (Example 3.2) boundary layers, 1D viscous Burgers equations with an inner layer (Example 3.3), two-dimensional (2D) steady-state convection-diffusion problems featuring two boundary layers (Example 3.4), and 2D Helmholtz problems characterized by oscillations acting as inner layers (Example 3.5). The numerical results indicate that the two-scale neural network method can provide reasonable accuracy in capturing features arising from large derivatives in solutions. These features include boundary layers, inner layers, and oscillations.

For all the numerical tests, we let $\gamma = -\frac{1}{2}$ (γ is defined in (1.2)). Without stating otherwise, we adopt the piecewise constant learning rates scheduler, the uniform distribution for collocation points, and the tan h activation function, as listed in Table 1. For some numerical tests, we employ the successive training strategy listed in Algorithm 1.

Example 3.1 (1D ODE with one boundary layer).

$$-\varepsilon u'' + 2u' = 3, \quad u(0) = 0, \quad u(1) = 0.$$

Learning Rates (η)	Collocation Points	Activation Function
≤ 10000 steps: $\eta = 10^{-3}$ (1D problems), $\eta = 10^{-2}$ (2D) 10000 to 30000 steps: $\eta = 5 \times 10^{-3}$ 30000 to 50000 steps: $\eta = 10^{-3}$ 50000 to 70000 steps: $\eta = 5 \times 10^{-4}$ ≥ 70000 steps: $\eta = 10^{-4}$	uniform distribution	tanh

TABLE 1. Learning rates scheduler, collocation points distribution, and activation function

The exact solution to this problem is

$$u(x) = \frac{3}{2} \left(x - \frac{\exp(-2(1-x)/\epsilon) - \exp(-2/\epsilon)}{1 - \exp(-2/\epsilon)} \right).$$

The solution has a boundary layer at $x = 1$. We use the two-scale neural networks $N(x, (0.5-x)/\sqrt{\epsilon}, 1/\sqrt{\epsilon})$ to solve the ODE problem. The neural network (NN) size is $(3, 20, 20, 20, 20, 1)$. We collect the numerical results in Figures 1 and 4(a) for the case where $\epsilon = 10^{-2}$. Observing from Figure 1(b) to (d), the NN solution matches the exact solution very well, with the relative errors around the boundary layer $x = 1$ only at the magnitude of 10^{-3} .

For the case where $\epsilon = 10^{-3}$, we collect the results in Figures 2 and 4(b). As depicted in Figure 2(a), the NN solution captures the behavior of the exact solution. While there is a relatively larger error observed very close to $x = 1$ as shown in Figure 2(b) and (c), it is essential to note that this challenge is inherent to the nature of the problem itself. In particular, when $\epsilon = 10^{-3}$, the boundary layer essentially takes the form of a vertical line. This results in a heightened sensitivity to the shift between the actual and predicted boundary layer in the vicinity of $x = 1$, as shown in Figure 2(c).

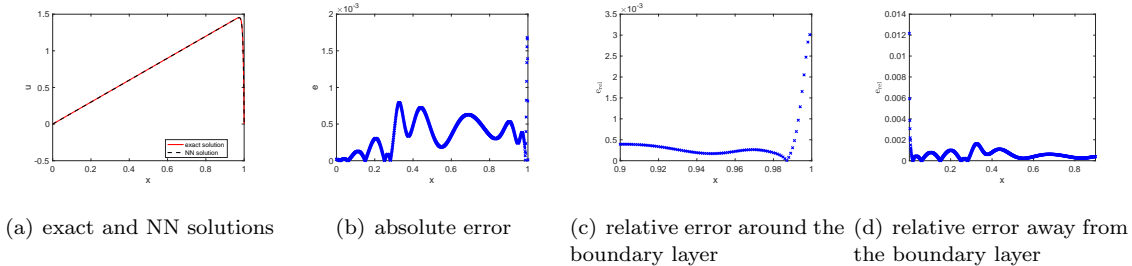


FIGURE 1. numerical results for Example 3.1 when $\epsilon = 10^{-2}$ using $N(x, (0.5 - x)/\sqrt{\epsilon}, 1/\sqrt{\epsilon})$, $\alpha = 1, \alpha_1 = 0, N_c = 200, \text{epoch} = 20000$.

Example 3.2 (1D ODE with two boundary layers).

$$(3.1) \quad \epsilon u'' - xu' - u = 0, \quad -1 < x < 1, \quad u(-1) = 1, \quad u(1) = 2.$$

The exact solution to the problem is

$$\exp\left(\frac{x^2 - 1}{2\epsilon}\right) \frac{\text{Erf}\left(\frac{x}{\sqrt{2\epsilon}}\right) + 3\text{Erf}\left(\frac{1}{\sqrt{2\epsilon}}\right)}{2\text{Erf}\left(\frac{1}{\sqrt{2\epsilon}}\right)}, \quad \text{Erf}(z) = \frac{2}{\sqrt{\pi}} \int_0^z \exp(-t^2) dt.$$

The solution has two boundary layers, at $x = \pm 1$.

We solve the considered problem using the two-scale NN $N(x, x/\sqrt{\epsilon}, 1/\sqrt{\epsilon})$. The NN size is $(3, 20, 20, 20, 20, 1)$. We collect the numerical results in Figures 3 and 4(c) for the case when $\epsilon = 10^{-2}$. The figures illustrate the excellent agreement between the NN solution and the exact solution, even at the boundary layers. As shown in Figure 3(c) and (d), the relative error is at the level of 10^{-2} in the vicinity of the left boundary

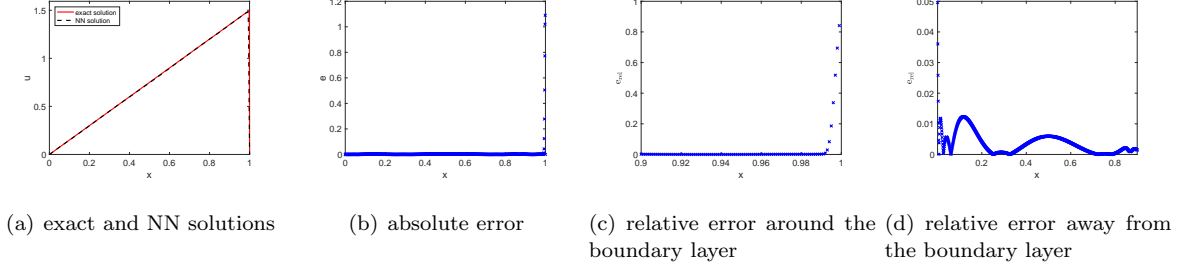


FIGURE 2. numerical results for Example 3.1 when $\epsilon = 10^{-3}$, using $N(x, (0.5 - x)/\sqrt{\epsilon}, 1/\sqrt{\epsilon})$, $\alpha = 1000$, $\alpha_1 = 10^{-6}$, $N_c = 450$, epoch=25000.

layer and around 10^{-3} near the right boundary layer. These results underscore the capability of the two-scale NN method in capturing multiple boundary layers in the exact solution.

For the scenario when $\epsilon = 10^{-3}$, the boundary layers practically become vertical lines, as shown in Figure 5(a). To address this inherent difficulty, we adopt the successive training strategy outlined in Algorithm 1. To be specific, we initialize the parameters (weights and biases) of $N\left(x, \frac{x}{\sqrt{\epsilon}}, \frac{1}{\sqrt{\epsilon}}\right)$ when $\epsilon = 10^{-3}$ using the pre-trained parameters obtained from training with $\epsilon = 10^{-2}$. We collect the results in Figure 5. While the NN solution does not achieve the same level of precision as when $\epsilon = 10^{-2}$, it is crucial to note that this discrepancy is primarily due to the inherent difficulty of the problem itself: the two boundary layers essentially become vertical lines. Despite the challenge, the two-scale NN solution still captures the key features of the exact solution, as shown in Figure 5(a). In addition, we provide a visualization of the shift between the actual and predicted solutions in Figure 5(c) and (d), illustrating that the shift occurs within a very narrow band around the right boundary.

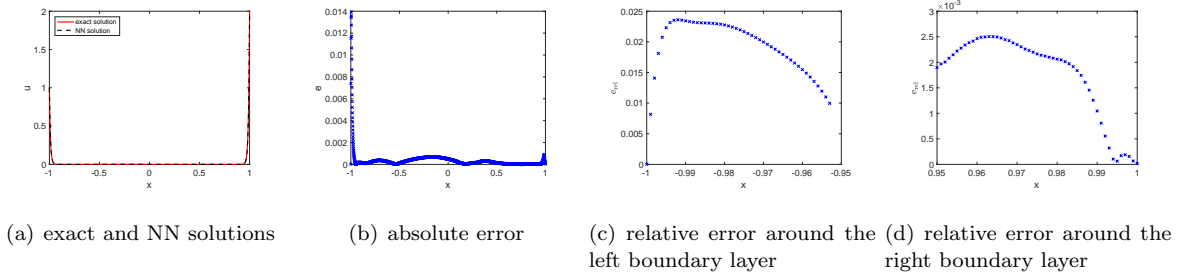


FIGURE 3. numerical results for Example 3.2 when $\epsilon = 10^{-2}$, using $N(x, x/\sqrt{\epsilon}, 1/\sqrt{\epsilon})$, $\alpha = 1$, $\alpha_1 = 0$, $N_c = 500$, epoch=20000.

Example 3.3 (1D viscous Burgers' equation).

$$(3.2) \quad \partial_t u + uu_x - \epsilon u_{xx} = 0$$

with initial conditions: $u(0, x) = -\sin(\pi(x - x_0))$ and boundary conditions $u(t, -1) = u(t, 1) = g(t)$, where $g(t)$ is determined from the exact solution

$$(3.3) \quad u(x, t) = -2\epsilon \frac{\partial_x v}{v}, \quad \text{where } v = \int_{\mathbb{R}} \exp\left(-\frac{\cos\left(\pi(x - x_0 - 2\sqrt{\epsilon}ts)\right)}{2\pi\epsilon}\right) e^{-s^2} ds.$$

We employ the two-scale NN that enforces the Dirichlet boundary condition, i.e., $(x^2 - 1)N(t, x, x/\sqrt{\epsilon}, 1/\sqrt{\epsilon}) + g(t)$ to solve the Burger's equation under a small viscosity parameter ϵ . The NN size is (4, 20, 20, 20, 20, 1).

First, we discuss the case when $\epsilon = 10^{-2}/\pi$. For $x_0 = 0$, i.e., the inner layer (nearly a shock profile) is located at the center of the domain. According to (3.3), $x_0 = 0$ leads to $g(t) = 0$. We employ the

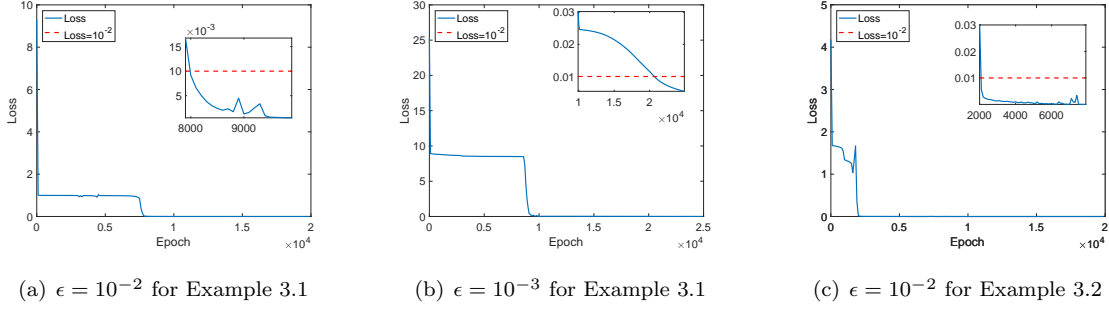


FIGURE 4. left: full and truncated loss history for Example 3.1 when $\epsilon = 10^{-2}$ and $\epsilon = 10^{-3}$, and for Example 3.2 when $\epsilon = 10^{-2}$. The configurations for these three cases are described in Figures 1, 2, and 3, respectively.

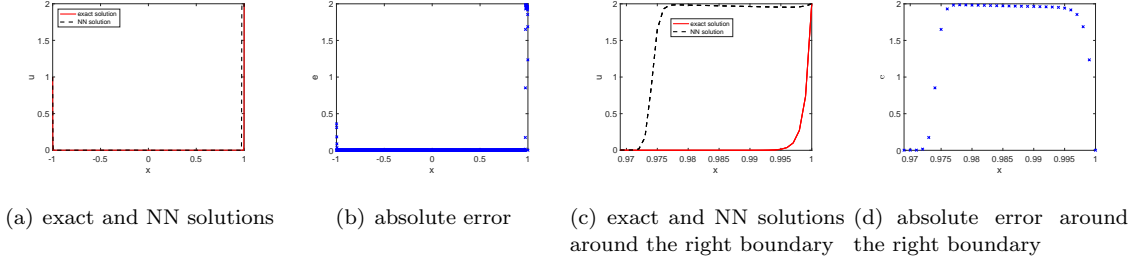


FIGURE 5. numerical results for Example 3.2 when $\epsilon = 10^{-3}$ using $N(x, x/\sqrt{\epsilon}, 1/\sqrt{\epsilon})$, $\alpha = 1, \alpha_1 = 10^{-4}$ when $\epsilon = 10^{-3}$, $N_c = 430$, epoch=50000. The parameters of the NN are pre-trained using $N(x, x/\sqrt{\epsilon}, 1/\sqrt{\epsilon})$ with $\epsilon = 10^{-2}$, with *constant learning rate* 10^{-3} , $\alpha = 1, \alpha_1 = 0$, $N_c = 500$, epoch=30000.

successive training strategy in Algorithm 1 by initializing the parameters of this NN using the pre-trained parameters obtained from training with $\epsilon = 10^{-1}/\pi$. We collect the numerical results in Figure 6. From Figure 6(e), we can see that the maximal relative error at the final time node $t = 1$ is 2.5%. The absolute error around the inner layer, i.e., around $x = 0$, is only at the level of 10^{-3} , which accounts for a mere 0.4% of the amplitude of the inner layer.

In the scenario where the inner layer is not at the center of the domain, i.e., $x_0 = 0.5$, we collect the results in Figures 6(b), (f), (g), (h) and (i), indicating an excellent agreement between the NN and exact solutions. We can see that the maximal relative error at the final time node $t = 1$ is within 0.6%, and the absolute error around $x = 0.5$ is at the level of 10^{-2} , representing only 1% of the amplitude of the inner layer. The results indicate that the two-scale NN method can accurately capture the exact solution of the Burgers' equation when $\epsilon = 10^{-2}/\pi$, regardless of whether the inner layer is near the center of the spatial domain or not.

When $\epsilon = 10^{-3}/\pi$, it is difficult to achieve accurate numerical quadrature for the exact solution in (3.3) because the integrand can vary from tiny scales to infinity, driven by the very small ϵ . Therefore, we employ the high-resolution finite element solution as the reference solution. The NN solution is obtained through a two-phase successive training process with Algorithm 1. To be specific, we initialize the NN parameters with the pre-trained parameters obtained from training with $\epsilon = 10^{-2}/\pi$. These pre-trained parameters themselves were initially obtained from the training process with $\epsilon = 10^{-1}/\pi$. As observed in Figure 7, there is a shift between the exact solution and the predicted solution by the two-scale NN method within a very narrow band around the inner layer at $x = 0$. The observed deviation primarily arises from the inherent difficulty of the problem itself. Indeed, given $\epsilon = 10^{-3}/\pi$, the inner

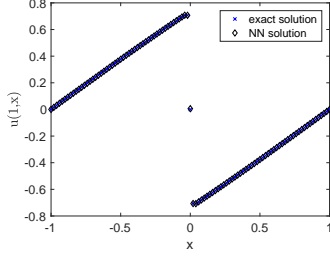
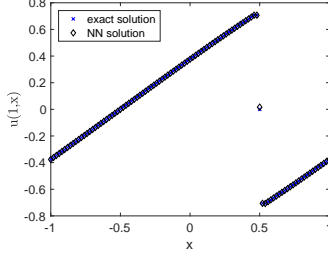
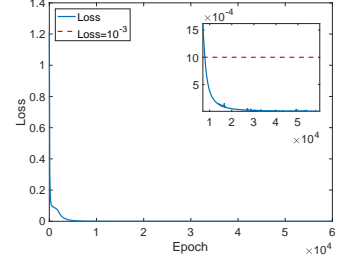
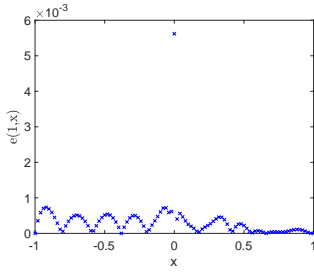
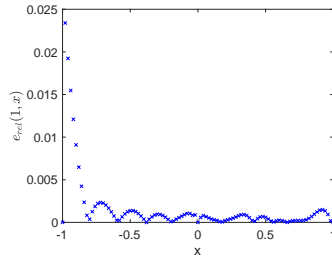
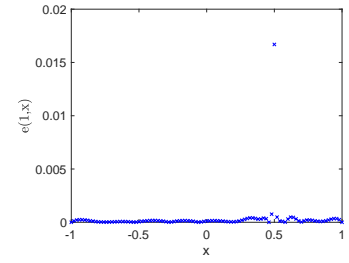
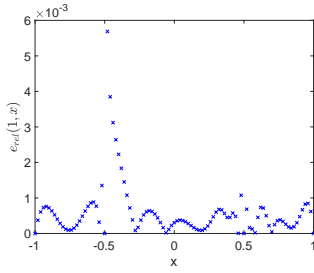
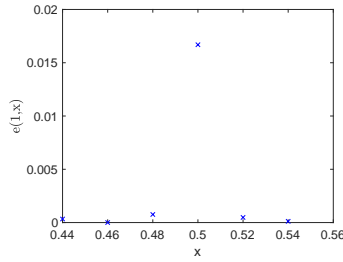
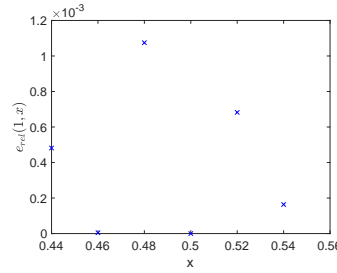
(a) exact and NN solutions when $x_0 = 0$ (b) exact and NN solutions when $x_0 = 0.5$ (c) full and truncated loss history when $x_0 = 0$ (d) absolute error when $x_0 = 0$ (e) relative error when $x_0 = 0$ (f) absolute error when $x_0 = 0.5$ (g) relative error when $x_0 = 0.5$ (h) absolute error around $x = 0.5$ when $x_0 = 0.5$ (i) relative error around $x = 0.5$ when $x_0 = 0.5$

FIGURE 6. numerical results for Example 3.3 when $\epsilon = 10^{-2}/\pi$ using $(x^2 - 1)N(t, x, x/\sqrt{\epsilon}, 1/\sqrt{\epsilon}) + g(t)$ at $t = 1$. $\alpha = 1, \alpha_1 = 0, N_c = 22500$ on the plane (t, x) , epoch=60000, with constant learning rate 10^{-4} (pre-trained with $\epsilon = 10^{-1}/\pi$, epoch=30000). The relative error is set to zero at $x = -1, 0, 1$ (when $x_0 = 0$) and at $x = \pm 0.5$ (when $x_0 = 0.5$), where $|u(1, x)| < 10^{-14}$.

layer practically becomes a vertical line. Nevertheless, the two-scale NN solution still captures the key features of the exact solution in this context.

Example 3.4 (2D steady-state convection-diffusion problem).

$$\begin{aligned} -\epsilon \Delta u + (u_x + u_y) &= f \text{ in } \Omega = (0, 1)^2, \\ u &= 0 \text{ on } \partial\Omega. \end{aligned}$$

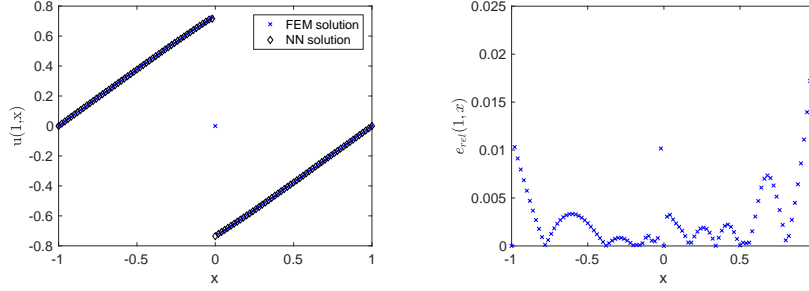


FIGURE 7. **left:** high resolution FEM solution with mesh size $1/500$, polynomial degree 2 and NN solution obtained with $N(t, x, x/\sqrt{\epsilon}, 1/\sqrt{\epsilon})$ for Example 3.3 when $\epsilon = 10^{-3}/\pi$, $x_0 = 0$ at $t = 1$. $\alpha = 1$, $N_c = 22500$ on the plane (t, x) , epoch=60000 (two-phase successive training: pre-trained with $\epsilon = 10^{-2}/\pi$, epoch=60000; the pre-trained parameters are obtained from training with $\epsilon = 10^{-1}/\pi$, epoch=30000); **right:** relative error.

The exact solution is given by: $u = xy \left(1 - \exp\left(-\frac{1-x}{\epsilon}\right)\right) \left(1 - \exp\left(-\frac{1-y}{\epsilon}\right)\right)$, and the right-hand side function is then:

$$f = (x+y) \left(1 - \exp\left(-\frac{1-x}{\epsilon}\right) \exp\left(-\frac{1-y}{\epsilon}\right)\right) + (x-y) \left(\exp\left(-\frac{1-y}{\epsilon}\right) - \exp\left(-\frac{1-x}{\epsilon}\right)\right).$$

According to [43], the exact solution has two boundary layers around the outflow boundaries $x = 1$ and $y = 1$. The two-scale NN we employ here is $N(x, (0.5-x)/\sqrt{\epsilon}, 1/\sqrt{\epsilon}, y, (0.5-y)/\sqrt{\epsilon}, 1/\sqrt{\epsilon})$, with the size $(6, 64, 64, 64, 1)$. The numerical results are collected in Figure 8 for $\epsilon = 10^{-2}$. The figures demonstrate that the NN solution accurately captures the exact solution, including the two boundary layers $x = 1$ and $y = 1$. Specifically, in Figure 8(h), we observe that the relative error around these boundary layers remains below 0.8%.

It is important to note that the challenge posed by this problem extends beyond the presence of boundary layers. Another critical aspect lies in the rapid variation of the right-hand-side function f , occurring at $x = 1$ and $y = 1$, as illustrated in Figure 8(a). Even so, the prediction by the two-scale NN method is accurate.

Example 3.5 (2D Helmholtz problem). Consider the boundary value problem

$$\begin{aligned} -\Delta u - k^2 u &= f & \text{in } \Omega = (-1, 1)^2 \\ u &= g & \text{on } \partial\Omega. \end{aligned}$$

We consider the following two cases where the exact solutions are respectively given by

$$\begin{aligned} a) \quad & u = \sin(a_1 \pi x) \sin(a_2 \pi y). \\ b) \quad & u = \frac{\cos(kr)}{k} - \frac{J_0(kr)(J_0(k) \cos k + J_1(k) \sin k)}{k(J_0^2(k) + J_1^2(k))}, \end{aligned}$$

where $r = \sqrt{x^2 + y^2}$, $J_\nu(\cdot)$ are Bessel functions of the first kind. These two cases represent the oscillation pattern of the solutions in the $x - y$ direction and the radial direction, respectively.

For **Example 3.5 a)**, we take $\epsilon = 1/\max\{a_1, a_2\}$. In this regard, we address the Helmholtz problem numerically in two scenarios. First, we set $(a_1, a_2) = (1, 4)$, which corresponds to a modest derivative in the solution and a relatively lower frequency for the time-harmonic wave. Secondly, we consider the case of $(a_1, a_2) = (2, 3)$, representing a larger derivative in the solution and a higher frequency for the wave. We employ a two-scale NN framework $(x^2 - 1)(y^2 - 1)N(x, x/\sqrt{\epsilon}, 1/\sqrt{\epsilon}, y, y/\sqrt{\epsilon}, 1/\sqrt{\epsilon})$, where we enforce the homogeneous Dirichlet boundary condition by the construction of the NN. The size of the

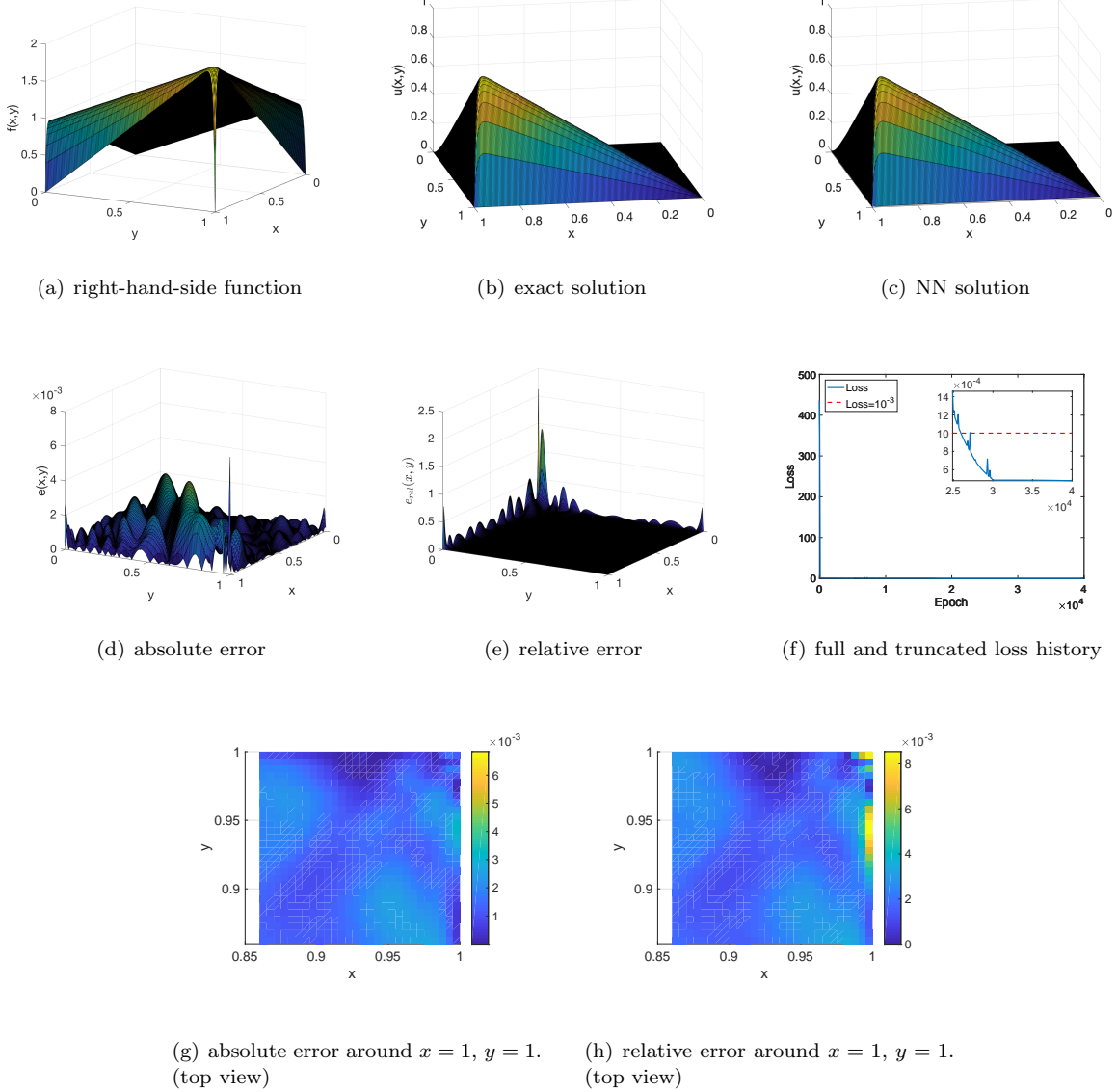


FIGURE 8. numerical results for Example 3.4 when $\epsilon = 10^{-2}$ using $N(x, (0.5 - x)/\sqrt{\epsilon}, 1/\sqrt{\epsilon}, y, (0.5 - y)/\sqrt{\epsilon}, 1/\sqrt{\epsilon})$ with $\alpha = 100, \alpha_1 = 0, N_c = 22500, \text{epoch} = 35000$. We enforce $e_{rel}(x, y) = 0$ on $\partial\Omega$ where the exact solution $u = 0$. The relative l^2 error is $e_{rel}^{l^2} = 1.5722 \times 10^{-5}$.

NN is $(6, 10, 10, 10, 10, 1)$. The results are collected in Figure 9. Observing from Figure 9(a), (b), (d), and (e), the NN solution matches the exact solution well.

As a comparison to the two-scale NN solution, when $(a_1, a_2) = (1, 4)$, we present the solution obtained by the one-scale NN, i.e., $(x^2 - 1)(y^2 - 1)N(x, y)$ in Figure 9(c), with NN size $(2, 10, 10, 10, 10, 1)$. The figure shows that the one-scale NN solution fails to capture the oscillation pattern in the exact solution and deviates significantly from the expected outcome.

We also compare the two-scale NN solutions to those from multi-level neural networks [1], known for their capability to address high-frequency issues. In the multi-level neural network method, a critical technique for addressing high-frequency issues involves scaling the equation's source term with a factor.

To be specific, at the initial neural network level, u_0 is solved from the equation with a scaling factor μ_0 : $R_0(x, u_0) = \mu_0 f - \mathcal{L}u_0 = 0$. The NN solution to this equation is denoted as \tilde{u}_0 , resulting in the initial approximation $\tilde{u} = \tilde{u}_0/\mu_0$. In the subsequent i -th level ($i \geq 1$) of the neural network, u_i is solved from $R_i(x, u_i) = \mu_i R_{i-1}(x, \tilde{u}_{i-1}) - \mathcal{L}u_i = 0$. The NN solution for this level is denoted as \tilde{u}_i . The updated approximation is then obtained by summing the initial approximation with the cumulative corrections

up to the i -th level, i.e., $\tilde{u} = \sum_{i=0}^L \frac{\tilde{u}_i}{\prod_{k=0}^i \mu_k}$. For more details of the algorithm of the multi-level neural networks, we refer the readers to Section 4 of [1].

We specifically investigate the case $(a_1, a_2) = (1, 4)$ with the multi-level neural networks. The hyper-parameters used for multi-level NN are summarized in Table 2, which are suggested in [1] for 2D numerical examples. The networks are first trained with Adam, followed by refinement with L-BFGS. We note that [1] does not explicitly specify how to select the initial scaling factor μ_0 ; nonetheless, we choose $\mu_0 = \max_{x \in \Omega} |f(x)|$. For the subsequent levels, according to [1], we choose μ_i ($i \geq 1$) to be the inverse of the amplitude of a rough approximation of \tilde{u}_i by extreme learning machine [13] (where only the weights and biases of the output layer are updated) is of order 1. As a result, as shown in Figure 10 (left), we find that the approximation by the initial layer $\tilde{u} = \tilde{u}_0/\mu_0$ is comparable to the ones using our two-scale NN method (shown in Figure 9(d)). However, as shown in Figure 10 (right), the approximation with the correction by the first level $\tilde{u} = \tilde{u}_0/\mu_0 + \tilde{u}_1/(\mu_0\mu_1)$ does not improve the accuracy. Similar phenomena are observed for $(a_1, a_2) = (2, 3)$. We also discover that the results of multi-level NN are highly sensitive to scaling factors. Nevertheless, this comparison underscores the critical role of scaling—whether applied to the equation or the neural networks—in addressing high-frequency issues.

Hyper-parameters	\tilde{u}_0	\tilde{u}_1
# Hidden layers	2	2
Widths of each hidden layer	10	20
# Adam iterations	2500	5000
# L-BFGS iterations	200	400

TABLE 2. Hyper-parameters used in Example 3.5 a) with multi-level neural networks [1]

For **Example 3.5 b)**, to avoid evaluating singular derivatives of the solution, we exclude the sampling points close to the origin. To utilize NN solutions that can exactly enforce the Dirichlet boundary condition for the problem, we consider the following auxiliary problem:

$$(3.4) \quad \begin{aligned} -\Delta \tilde{u} - k^2 \tilde{u} &= f \quad \text{in } \Omega = (-1, 1)^2, \\ \tilde{u} &= 0 \quad \text{on } \partial\Omega. \end{aligned}$$

Then $u = \tilde{u} + g_b$, where g_b is defined to be

$$g_b(x, y) = x^2(g_2(y) - g(1, 1)) + y^2(g_1(x) - g(1, 1)) + g(1, 1),$$

with $g_2(y) = g(1, y)$, $g_1(x) = g(x, 1)$. Taking $\epsilon = 1/k^2$, we utilize the neural networks $(x^2 - 1)(y^2 - 1)N(x, x/\sqrt{\epsilon}, y, 1/\sqrt{\epsilon}, y/\sqrt{\epsilon}, 1/\sqrt{\epsilon})$ to solve the auxiliary problem (3.4) and, consequently, obtain the solution u to the original Helmholtz problem. We collect the numerical results in Figure 12. The figure demonstrates that the two-scale NN solution accurately captures the radial oscillation pattern for a modest wave number $k = 10$, an achievement the corresponding one-scale approach does not replicate under the same configuration.

4. CONCLUSION AND DISCUSSION

In this work, we construct the two-scale neural networks by explicitly incorporating small parameters in partial differential equations into the architecture of feedforward neural networks. The construction enables solving problems with small parameters in a simple fashion, without modifying the formulations

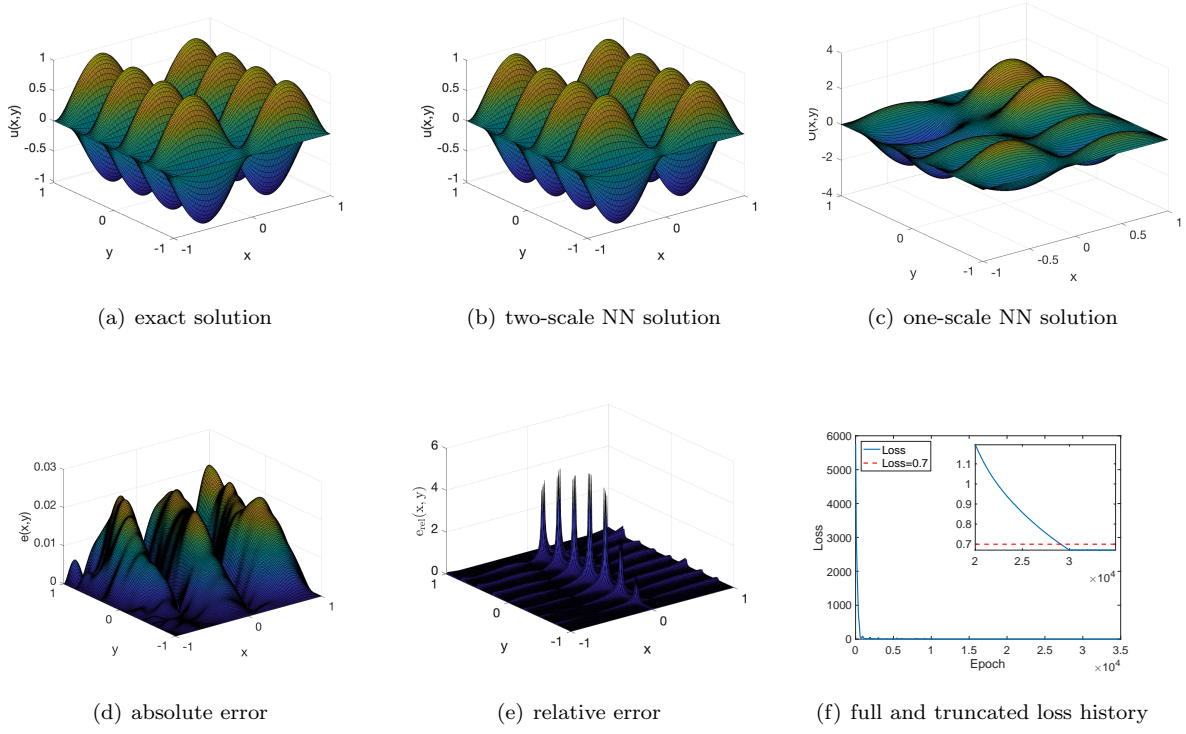


FIGURE 9. (b)(d)(e)(f) are numerical results with the two-scale NN for Example 3.5 a), when $k = 4, a_1 = 1, a_2 = 4$ using $(x^2 - 1)(y^2 - 1)N(x, x/\sqrt{\epsilon}, 1/\sqrt{\epsilon}, y, y/\sqrt{\epsilon}, 1/\sqrt{\epsilon})$, $\alpha = 1, \alpha_1 = 0, N_c = 22500$, epoch=40000. We enforce $e_{rel}(x, y) = 0$ on the nodes where the exact solution $u = 0$. The relative l^2 error: $e_{l^2}^{rel} = 5.2195 \times 10^{-4}$. (c) is the numerical result with the one-scale NN, using $(x^2 - 1)(y^2 - 1)N(x, y)$, the other configurations are the same as the two-scale method.

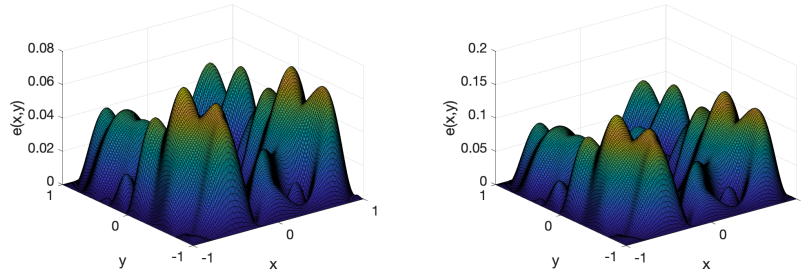


FIGURE 10. absolute error between exact solution and left: $\tilde{u} = \tilde{u}_0/\mu_0$; right: $\tilde{u} = \tilde{u}_0/\mu_0 + \tilde{u}_1/(\mu_0\mu_1)$ for Example 3.5 a) when $k = 4, a_1 = 1, a_2 = 4$ using $(x^2 - 1)(y^2 - 1)N(x, y)$. $\alpha = 1, \alpha_1 = 0, N_c = 22500$, using multi-level neural networks with hyper-parameters specified in Table 2.

of PINNs or adding Fourier features in the networks. Extensive numerical tests illustrate that the two-scale neural network method is effective and provides reasonable accuracy in capturing features associated with large derivatives in solutions. These features include boundary layers, inner layers, and oscillations.

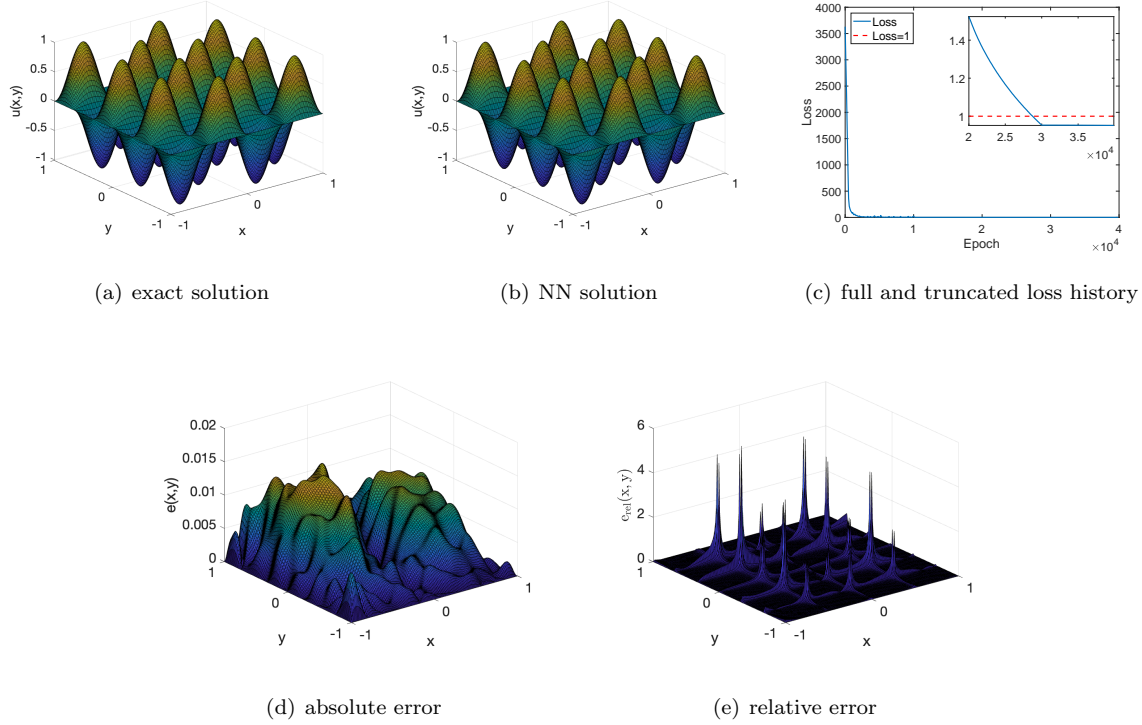


FIGURE 11. numerical results for Example 3.5 a), when $k = 3$, $a_1 = 2$, $a_2 = 3$ using $(x^2 - 1)(y^2 - 1)N(x, x/\sqrt{\epsilon}, 1/\sqrt{\epsilon}, y, y/\sqrt{\epsilon}, 1/\sqrt{\epsilon})$, $\alpha = 1$, $\alpha_1 = 0$, $N_c = 22500$, epoch=40000. We enforce $e_{rel}(x, y) = 0$ on the nodes where the exact solution $u = 0$. The relative l^2 error: $e_{l^2}^{rel} = 5.2195 \times 10^{-4}$.

Notably, when a parameter in the differential equations becomes extremely small, the method struggles to accurately capture large derivatives. However, for problems with extremely small parameters, the proposed two-scale neural network method may be employed as a good initial guess for further training.

ACKNOWLEDGEMENT

We thank Mr. Ziad Aldirany from Polytechnique Montréal for providing the code for multi-level neural networks, which we utilized in comparing our results. GEK acknowledges support by the DOE SEA-CROGS project (DE-SC0023191) and the MURI-AFOSR project (FA9550-20-1-0358).

REFERENCES

- [1] Ziad Aldirany, Régis Cottureau, Marc Laforest, and Serge Prudhomme. Multi-level neural networks for accurate solutions of boundary-value problems. *Comput. Methods Appl. Mech. Engrg.*, 419:116666, 2024.
- [2] Sokratis J. Anagnostopoulos, Juan Diego Toscano, Nikolaos Stergiopoulos, and George Em Karniadakis. Residual-based attention and connection to information bottleneck theory in PINNs. *Comput. Methods Appl. Mech. Engrg.*, 421:116805, 2024.
- [3] Ronen Basri, Meirav Galun, Amnon Geifman, David Jacobs, Yoni Kasten, and Shira Kritchman. Frequency bias in neural networks for input of non-uniform density. *arXiv:2003.04560*, 2020.
- [4] Giulia Bertaglia, Chuan Lu, Lorenzo Pareschi, and Xueyu Zhu. Asymptotic-preserving neural networks for multiscale hyperbolic models of epidemic spread. *Math. Models Methods Appl. Sci.*, 32(10):1949–1985, 2022.
- [5] Wei Cai, Xiaoguang Li, and Lizuo Liu. A phase shift deep neural network for high frequency approximation and wave problems. *SIAM J. Sci. Comput.*, 42(5):A3285–A3312, 2020.
- [6] Wojciech M. Czarnecki, Simon Osindero, Max Jaderberg, Grzegorz Swirszcz, and Razvan Pascanu. Sobolev training for neural networks. In I. Guyon, U. Von Luxburg, S. Bengio, H. Wallach, R. Fergus, S. Vishwanathan, and R. Garnett, editors, *Adv. Neural Inf. Process. Syst.*, volume 30. Curran Associates, Inc., 2017.

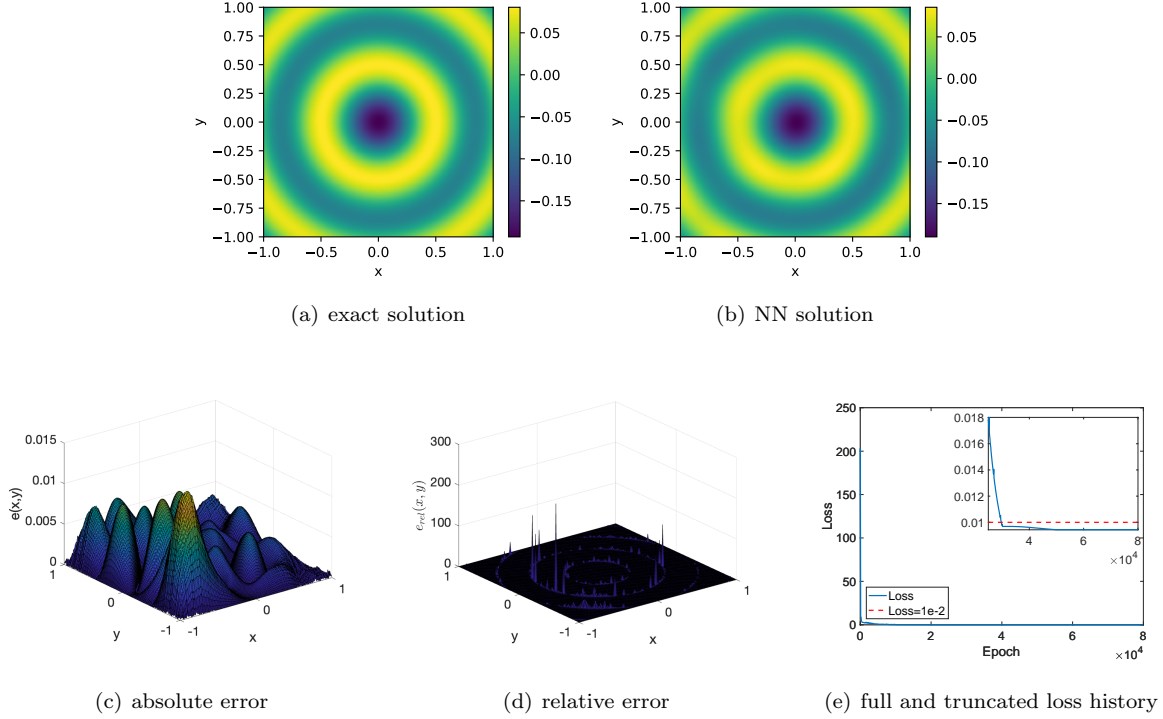


FIGURE 12. numerical results for Example 3.5 b) when $k = 10$ using $(x^2 - 1)(y^2 - 1)N(x, x/\sqrt{\epsilon}, y, 1/\sqrt{\epsilon}, y/\sqrt{\epsilon}, 1/\sqrt{\epsilon})$ with $k = 1/\sqrt{\epsilon}$, $\alpha = 1$, $\alpha_1 = 0$, $N_c = 22497$, epoch=80000. The relative l^2 error is: $e_{l^2}^{rel} = 3.72 \times 10^{-3}$.

- [7] Zhiwei Fang, Sifan Wang, and Paris Perdikaris. Ensemble learning for physics informed neural networks: a gradient boosting approach. *arXiv:2302.13143*, 2023.
- [8] Zhiwei Gao, Tao Tang, Liang Yan, and Tao Zhou. Failure-informed adaptive sampling for PINNs, part ii: combining with re-sampling and subset simulation. *arXiv preprint arXiv:2302.01529*, 2023.
- [9] Zhiwei Gao, Liang Yan, and Tao Zhou. Failure-informed adaptive sampling for PINNs. *SIAM J. Sci. Comput.*, 45(4):A1971–A1994, 2023.
- [10] Yiqi Gu, Haizhao Yang, and Chao Zhou. SelectNet: self-paced learning for high-dimensional partial differential equations. *J. Comput. Phys.*, 441:Paper No. 110444, 18, 2021.
- [11] Weiling Guan, Kaihan Yang, Yinsheng Chen, Shaolin Liao, and Zhong Guan. A dimension-augmented physics-informed neural network (DaPINN) with high level accuracy and efficiency. *J. Comput. Phys.*, 491:Paper No. 112360, 2023.
- [12] Judy Hoffman, Daniel A. Roberts, and Sho Yaida. Robust learning with Jacobian regularization, 2020.
- [13] Guang-Bin Huang, Dian Wang, and Yuan Lan. Extreme learning machines: a survey. *Int. J. Mach. Learn. Cybern.*, 2:107–122, 06 2011.
- [14] Ameya D Jagtap, Kenji Kawaguchi, and George Em Karniadakis. Adaptive activation functions accelerate convergence in deep and physics-informed neural networks. *J. Comput. Phys.*, 404:109136, 2020.
- [15] Shi Jin, Zheng Ma, and Keke Wu. Asymptotic-preserving neural networks for multiscale time-dependent linear transport equations. *J. Sci. Comput.*, 94(3):Paper No. 57, 21, 2023.
- [16] Diederik P Kingma and Jimmy Ba. Adam: A method for stochastic optimization. *arXiv:1412.6980*, 2014.
- [17] Sven Lämmle, Can Bogoclu, Kevin Cremanns, and Dirk Roos. Gradient and uncertainty enhanced sequential sampling for global fit. *Comput. Methods Appl. Mech. Engrg.*, 415:Paper No. 116226, 23, 2023.
- [18] Xi-An Li, Zhi-Qin John Xu, and Lei Zhang. A multi-scale DNN algorithm for nonlinear elliptic equations with multiple scales. *Commun. Comput. Phys.*, 28(5):1886–1906, 2020.
- [19] Xi-An Li, Zhi-Qin John Xu, and Lei Zhang. Subspace decomposition based DNN algorithm for elliptic type multi-scale PDEs. *J. Comput. Phys.*, 488:Paper No. 112242, 17, 2023.
- [20] Ziqi Liu, Wei Cai, and Zhi-Qin John Xu. Multi-scale deep neural network (MscaledNN) for solving Poisson-Boltzmann equation in complex domains. *Commun. Comput. Phys.*, 28(5):1970–2001, 2020.
- [21] Lu Lu, Xuhui Meng, Zhiping Mao, and George Em Karniadakis. Deepxde: A deep learning library for solving differential equations. *SIAM Review*, 63(1):208–228, 2021.

- [22] Yulong Lu, Li Wang, and Wuzhe Xu. Solving multiscale steady radiative transfer equation using neural networks with uniform stability. *Res. Math. Sci.*, 9(3):45, 2022.
- [23] Suryanarayana Maddu, Dominik Sturm, Christian L Müller, and Ivo F Sbalzarini. Inverse dirichlet weighting enables reliable training of physics informed neural networks. *Mach. Learn.: Sci. Technol.*, 3(1):015026, 2022.
- [24] Levi D. McClenny and Ulisses M. Braga-Neto. Self-adaptive physics-informed neural networks. *J. Comput. Phys.*, 474:Paper No. 111722, 23, 2023.
- [25] Mohammad Amin Nabian, Rini Jasmine Gladstone, and Hadi Meidani. Efficient training of physics-informed neural networks via importance sampling. *CoRR*, abs/2104.12325, 2021.
- [26] Nasim Rahaman, Aristide Baratin, Devansh Arpit, Felix Draxler, Min Lin, Fred Hamprecht, Yoshua Bengio, and Aaron Courville. On the spectral bias of neural networks. In *International Conference on Machine Learning*, pages 5301–5310, 2019.
- [27] Hans-Görg Roos, Martin Stynes, and Lutz Tobiska. *Robust Numerical Methods for Singularly Perturbed Differential Equations*. Springer, 2008.
- [28] Hwijae Son, Jin Woo Jang, Woo Jin Han, and Hyung Ju Hwang. Sobolev training for physics informed neural networks. *Commun. Math. Sci.*, 21(6):1679–1705, 2023.
- [29] Kejun Tang, Xiaoliang Wan, and Chao Yang. DAS-PINNs: a deep adaptive sampling method for solving high-dimensional partial differential equations. *J. Comput. Phys.*, 476:Paper No. 111868, 26, 2023.
- [30] Kejun Tang, Jiayu Zhai, Xiaoliang Wan, and Chao Yang. Adversarial adaptive sampling: Unify PINN and optimal transport for the approximation of PDEs. 2023.
- [31] Bo Wang, Wenzhong Zhang, and Wei Cai. Multi-scale deep neural network (MscaleDNN) methods for oscillatory Stokes flows in complex domains. *Commun. Comput. Phys.*, 28(5):2139–2157, 2020.
- [32] Sifan Wang, Shyam Sankaran, and Paris Perdikaris. Respecting causality is all you need for training physics-informed neural networks. *Comput. Methods Appl. Mech. Engrg.*, 421:116813, 2024.
- [33] Sifan Wang, Shyam Sankaran, Hanwen Wang, and Paris Perdikaris. An expert’s guide to training physics-informed neural networks. *arXiv:2308.08468*, 2023.
- [34] Sifan Wang, Hanwen Wang, and Paris Perdikaris. On the eigenvector bias of Fourier feature networks: from regression to solving multi-scale PDEs with physics-informed neural networks. *Comput. Methods Appl. Mech. Engrg.*, 384:Paper No. 113938, 28, 2021.
- [35] Sifan Wang, Hanwen Wang, and Paris Perdikaris. On the eigenvector bias of fourier feature networks: From regression to solving multi-scale PDEs with physics-informed neural networks. *Comput. Methods Appl. Mech. Engrg.*, 384:113938, 2021.
- [36] Chenxi Wu, Min Zhu, Qinyang Tan, Yadhu Kartha, and Lu Lu. A comprehensive study of non-adaptive and residual-based adaptive sampling for physics-informed neural networks. *Comput. Methods Appl. Mech. Engrg.*, 403:115671, 2023.
- [37] Zixue Xiang, Wei Peng, Xu Liu, and Wen Yao. Self-adaptive loss balanced physics-informed neural networks. *Neuro-computing*, 496:11–34, 2022.
- [38] Zhi-Qin John Xu, Yaoyu Zhang, Tao Luo, Yanyang Xiao, and Zheng Ma. Frequency principle: Fourier analysis sheds light on deep neural networks. *Commun. Comput. Phys.*, 28(5):1746–1767, 2020.
- [39] Andy L. Yang and Feng Gu. A mesh-less, ray-based deep neural network method for the Helmholtz equation with high frequency. *Int. J. Numer. Anal. Model.*, 19(4):587–601, 2022.
- [40] Jeremy Yu, Lu Lu, Xuhui Meng, and George Em Karniadakis. Gradient-enhanced physics-informed neural networks for forward and inverse PDE problems. *Comput. Methods Appl. Mech. Engrg.*, 393:Paper No. 114823, 22, 2022.
- [41] Guangtao Zhang, Huiyu Yang, Fang Zhu, Yang Chen, et al. Dasa-Pinns: Differentiable adversarial self-adaptive point-wise weighting scheme for physics-informed neural networks. *SSRN*, 2023.
- [42] Rui Zhang. Learning high frequency data via the coupled frequency predictor-corrector triangular DNN. *Jpn. J. Ind. Appl. Math.*, 40(2):1259–1285, 2023.
- [43] Zhimin Zhang. Finite element superconvergence on Shishkin mesh for 2-D convection-diffusion problems. *Math. Comp.*, 72(243):1147–1177, 2003.

(Qiao Zhuang) DEPARTMENT OF MATHEMATICAL SCIENCES, WORCESTER POLYTECHNIC INSTITUTE, WORCESTER, MA 01609, USA

Email address: qzhuang@wpi.edu

(Chris Ziyi Yao) DEPARTMENT OF AERONAUTICS, IMPERIAL COLLEGE LONDON, LONDON, SW7 2AZ, UK

Email address: chris.yao20@imperial.ac.uk

(Zhongqiang Zhang) DEPARTMENT OF MATHEMATICAL SCIENCES, WORCESTER POLYTECHNIC INSTITUTE, WORCESTER, MA 01609, USA

Email address: zzhang7@wpi.edu

(George Em Karniadakis) DIVISION OF APPLIED MATHEMATICS, BROWN UNIVERSITY, PROVIDENCE, RI 02912, USA

Email address: george_karniadakis@brown.edu